A THEORETICAL STUDY OF ICRF EFFECTS

ON MULTIPLE MIRROR CONFINEMENT

by

K. J. Doniger, M. A. Lieberman and A. J. Lichtenberg

A THEORETICAL STUDY OF ICRF EFFECTS
ON MULTIPLE MIRROR CONFINEMENT

by

K. J. Doniger, M. A. Lieberman and A. J. Lichtenberg

Department of Electrical Engineering and Computer Science,

University of California

Berkeley, CA 94720

We determine the improvements in a multiple mirror reactor system due to an asymmetrically applied ion cyclotron resonance field (ICRF). The resonance field is used to selectively reflect ions that travel away from the center of the device, thus creating a net ion drift towards the center. The ICRF effects in heating and scattering the ions and modifying the loss cone geometry are determined in detail. A one dimensional, non-ignited (finite $Q = fusion\ power/recirculating\ power$) model of a multiple mirror reactor is developed. Various scaling laws are numerically derived and compared to those of a symmetric system without ICRF. Radial diffusion due to classical collisions and ICRF effects is calculated. A 21 cell machine with a peak field of 280 kG and $Q = 5$ is reduced from 845 meters to 580 meters in length with the addition of the asymmetric ICRF. The total fusion power generated by the system is reduced from 8 Gwatts to 6.3 Gwatts.

I. Introduction

A multiple mirror fusion reactor consists of many magnetic mirror cells placed end to end along a linear axis. For the collisional regime in which the ion mean free path is of the order of a cell length, ions are continually trapped and retrapped in adjacent cells. The resulting random walk process along the axis yields an axial confinement time that scales as the square of the reactor length.[1-7] This scaling has been verified experimentally.[5,6] Multiple mirror plasmas have been stabilised using average-minimum-B fields,[8,9] and high β operation has been achieved.[10] A number of reactor feasibility design studies have been made,[11-14] including wetwood burner operation,[11] the effects of impurities,[11] high β radial diffusion,[12] and economic optimisations.[13,14] These studies show that although the diffusive scaling of the axial loss is favorable, overall reactor lengths tend to be long, of order 400-1200 meters.

In each cell of a normal multiple mirror, half of the particles retrap in the adjacent cell inwards (towards the center) and half retrap in the adjacent cell outwards (away from the center). In 1981, Post and Li[15] calculated the effects of changing these probabilities. The confinement time increases if it is more likely that a particle retraps inwards than outwards. Unfortunately, no mechanism to produce this *asymmetry* was investigated. In this paper, we study in detail one process that produces asymmetry: ion cyclotron resonance heating (ICRH). Under the particular conditions present in a multiple mirror system, and applied in the correct manner, ICRH reduces the volume of the outward facing loss cone in each cell.[16] This makes it more probable that particles escape inward. We show that this *loss cone asymmetry* greatly improves the parameters of a multiple mirror reactor, most notably by decreasing its length.

In Sec. II, the basic multiple mirror model is described. The effects of the ion cyclotron resonance field (ICRF) are determined in Sec. III. The calculation of the cell lengths is performed in Sec. IV. Numerical results of the power balance optimisation are presented in Sec. V. These include scaling laws, comparisons with previous studies, and the effects of radial diffusion.

II. The Basic Model

We consider a steady state system consisting of $2N + 1$ cells with an axis of symmetry through the midpoint of the central cell (see Fig. 1). To replace particles lost from the ends, there is a plasma source in the center of the system. The plasma consists of equal parts of deuterium and tritium nuclei, and their electrons. The length L of the system is assumed to be much greater than that of any individual cell (except, for reasons given later, the central cell). Each cell consists of a relatively long midplane region of constant magnetic field, and two short mirror regions where the field increases to its maximum value at the mirror throat. Note that the length and the magnetic field strength of a mirror cell need not be identical to that of its neighbors. The mirror ratio R in each cell is assumed to be large ($R^2 \gg 1$). In order to use the magnetic field efficiently, the value of midplane β and the value of the maximum vacuum magnetic field, B_{vM}, are made as large as possible and are uniform throughout the system. The maximum values of β and B_{vM} are determined by stability and engineering constraints that are beyond the scope of this paper.[13,17] The long, thin approximation is used throughout: $B(s) = B_z(s)$. Since the plasma pressure in cell j is $p_j = 2n_j T$, the constancy of β and B_{vM} gives

$$\left(R_j^2 + \frac{\beta}{1-\beta} \right) n_j = \text{const} , \qquad (1)$$

where n is the ion density and R is the *self consistent* mirror ratio, which differs from the vacuum mirror ratio due to finite β. Since the density decreases as one moves outward from the center to the ends, the mirror ratios increase and the midplane fields decrease (see Fig. 1).

Since magnetic flux is conserved, we have

$$\frac{A_j}{R_j} = \text{const} , \qquad (2)$$

where A_j is the plasma cross sectional area in cell j.

Unlike most magnetic fusion confinement schemes, the multiple mirror is collisional. Particles scatter into and out of the loss cone while moving axially through the system. When the mean free path of a particle is of the order of the cell length, particles are trapped and detrapped many times before escaping from the multiple mirror. This leads to random walk behavior along the length of the system, causing the particle confinement time to scale as the *square* of the system length. The high collisionality also thermalizes the plasma. Typically, the particle confinement time is an order of magnitude larger than the longest thermalization time. Coupled with high electron thermal conductivity, the plasma is considered to be a uniform temperature maxwellian throughout the system.

The 90° mean free path for an ion of velocity v scattering against a background ion distribution is[18]

$$\lambda(v) = K \frac{v^4}{n} , \qquad (3)$$

where K is a weak function of v. Equation (3) is used for a single ion species of mass 2.5 AMU because the two ion species (D and T) have similar masses, and because ion-electron scattering is negligible.

The mean free path for ion scattering through a loss cone angle is given by

$$\lambda^*(v) = \frac{\lambda(v)}{R} \ . \tag{4}$$

In a maxwellian plasma, all values of λ^* will be present. Ions can be divided into velocity classes based on the values of λ, λ^* and the various scale lengths. Very low velocity particles will have $\lambda \ll l_M$, the mirror scale length. Because the magnetic moment of single particles is not conserved in the mirror region, there is no mirror effect. The percentage of this class of particles is assumed to be negligible because due to the smallness of l_M . Very high velocity particles have mean free paths that satisfy $\lambda^* \gg L$. These particles are lost once they scatter into the loss cone. This class of particles is also negligible because of the exponential in the maxwellian velocity distribution.

Between these extremes lie the bulk of the particles, with $l_M \ll \lambda \ll RL$. This *intermediate mean free path* region was split into two parts by Makhijani et al.[7] Lower velocity particles that satisfy $\lambda^* \ll l_c$, where l_c is the length of a cell, are said to be in the *ideal multiple mirror* regime. Higher velocity particles with mean free paths such that $l_c \ll \lambda^* \ll L$ are in the *low density multiple mirror* regime. Particles in both regimes take random steps through the system, thus giving the diffusive (L^2) scaling. The ions in the low density regime take longer steps and are therefore lost more rapidly than those in the ideal regime. For this reason, it is desirable to adjust the cell lengths or λ^* such that the great majority of the ions are in the ideal regime. The ions in the low

density regime are then significant only in the calculation of the end loss power, because they are lost more quickly than ions in the ideal regime, and because they carry more than the average energy.

All other things being equal, the cost of a reactor system increases with length. To minimize this length, λ^* must be as small as possible. Thus, multiple mirrors operate at high mirror ratios ($R > 3$), low temperatures (5 keV) and high densities (10^{16} cm^{-3} in the central cell). Even so, the density is low near the ends of the system, and cells tend to be long there. Because $l_M \ll \lambda$, the mirror regions are collisionless, and particle motion is governed by conservation of energy and magnetic moment. The midplane regions and the system as a whole, however, are collisional because $\lambda^* \ll L$.

The only cell that is not governed by the value of λ^* is the central cell. Its length is determined by reactor power balance, not by particle trapping considerations. The optimized central cell length has been found[14] to comprise about half of the total system length.

Electrons play an important role in multiple mirror dynamics. Najmabadi et al.[19] made a careful study of ambipolar effects in a multiple mirror and found that the traditional correction factor,

$$1 + \langle Z \rangle \frac{T_e}{T_i} \approx 2 \,,$$

is reasonably accurate. In our model, this implies a 50 percent decrease in the ion confinement time.

In the steady state, the ion density in each cell is determined by particle conservation and the physics of trapping and detrapping in each cell. We assume that each cell contains a number of ions, H, and has ion fluxes F and G entering

and leaving (see Fig. 2). These quantities are linked by an average confinement time, τ. All of the ions are assumed to be in the ideal regime. This makes conditions in any cell dependent only on the adjacent cells, and it decouples the flux F_{j-1} from F_j, and G_j from G_{j-1}.

The continuity equations are

$$F_{j-1} = \frac{b_j^+}{b_j^- + b_j^+} \frac{H_j}{\tau_j},\tag{5a}$$

$$G_j = \frac{b_j^-}{b_j^- + b_j^+} \frac{H_j}{\tau_j},\tag{5b}$$

and

$$\frac{H_j}{\tau_j} = F_j + G_{j-1}.\tag{5c}$$

The quantities b_j^+ and b_j^- are defined as

$$b_j^+ = \frac{F_{j-1}}{F_j}, \qquad b_j^- = \frac{G_j}{G_j}$$

(see Fig. 2). The combinations of b_j^+ and b_j^- in (5a) and (5b) are the probabilities that a particle will *eventually* escape to the neighboring cell outward and inward, respectively.

Since no ions enter the system from the ends, we have

$$G_o = 0.\tag{6}$$

In the steady state, we have

$$F_j - G_j = F_o.\tag{7}$$

If all of the particles were in the ideal regime, the net outward flux throughout the system would be F_o. Numerically, the actual flux has been found[6,7] to be on the order of 5 percent larger for typical reactor designs.

Using equations (5) and (7), we eliminate H_j/τ_j, F_j and F_{j-1} to obtain

$$G_j = C_j(G_{j-1} + F_o) , \qquad (8)$$

where

$$C_j = \frac{b_j^-}{b_j^+} \qquad (9)$$

is the *asymmetry factor*. The improved confinement time due to asymmetry is caused by making C_j larger than unity.

The boundary condition (6) can be used to solve (8) for G_1 in terms of C_1 and F_o. This, in turn, can be used to solve (8) for G_2 in terms of C_1, C_2, and F_o, and so forth. The general solution for G_j is

$$G_j = \sigma_j F_o , \qquad (10)$$

where

$$\sigma_j = \sum_{i=1}^{j} \left(\prod_{k=i}^{j} C_k \right) .$$

To determine for the density in cell j, we must evaluate the flux

$$G_j = A_j n_j \int v_x f(\mathbf{v}) \, d\mathbf{v} ,$$

where $f(\mathbf{v})$ is the velocity distribution function. It has been shown[19] that the velocity due to the outward drift is much smaller than the thermal speed for all but, possibly, the last cell. Therefore, $f(\mathbf{v})$ is assumed to be a stationary maxwellian. The integral is taken over the inward facing loss cone in cell j. There is no ICRH at the inboard end of the cell, so the loss cone boundary is given by $\sin^2 \theta_{LC} = 1/R_j$. Evaluating the integral,

$$G_j = \frac{A_j n_j v_{th}}{2\sqrt{\pi} R_j} . \qquad (11)$$

We can eliminate G_j between (10) and (11) and solve for n_j. To account for the enhanced axial loss due to ambipolar effects, we must divide n_j by 2. The density in cell j is then

$$n_j = \frac{\sqrt{\pi}\,R_c}{v_{th}A_c}\,\sigma_j F_o \; , \qquad (12)$$

where (2) has been used to eliminate A_j, and the subscript "c" denotes a central cell quantity.

In the absence of asymmetry, $\sigma_j = 1$ for all j, and the density difference between adjacent cells is constant. If $C > 1$ and has the same value for all cells, the increment in density versus cell number will increase exponentially as one moves inwards.

The power flows in a multiple mirror reactor are shown in Fig. 3. Here, we are concerned only with power flow into and out of the plasma itself. In steady state, the power entering and leaving the plasma must be balanced,

$$P_L + P_\beta = f_1 P_F + P_R \; . \qquad (13)$$

The components of this power balance equation are explained in the following paragraphs.

The total fusion power is given by

$$P_F = \int_V W_F \langle \sigma v \rangle n_D n_T \, dx \; , \qquad (14)$$

where W_F is the energy generated by a single fusion event, $\langle \sigma v \rangle$ is the fusion reactivity, n_D and n_T are the densities of deuterium and tritium, and the integral is taken over the volume of the plasma. W_F is a constant and $\langle \sigma v \rangle$ is a function of temperature only; they can be removed from the integral. The densities of deuterium and tritium are equal to $n/2$. Since the mirror regions are very

short, almost all of the system volume consists of cell midplanes. The integral can therefore be approximated by a sum of midplane quantities. Equation (14) becomes

$$P_F = \frac{1}{4} W_F \langle \sigma v \rangle M , \qquad (15)$$

where

$$M = n_c^2 A_c l_c + 2 \sum_{j=1}^{N} n_j^2 A_j l_j . \qquad (16)$$

Alpha particles transfer a fraction $\sqrt{1 - 1/R_c}$ of their energy to the plasma via coulomb collisions.[14] Since alpha particles carry 20 percent of the fusion produced energy, the fraction of the fusion power absorbed directly by the plasma is

$$f_1 = \frac{1}{5} \sqrt{1 - 1/R_c} . $$

The power lost to bremsstrahlung is

$$P_\beta = \int_V k_\beta \sqrt{T} n_i n_e \, dx , \qquad (17)$$

where $k_\beta = 5.35 \cdot 10^{-37}$ watt/m^3-(keV)$^{1/2}$, n_i is the ion density and n_e is the electron density. Using the same approximations as before, (17) becomes

$$P_\beta = k_\beta \sqrt{T} M . \qquad (18)$$

The power lost axially is given by

$$P_L = 4 k_L T F_o . \qquad (19)$$

The factor of 4 comes from the two ends and the fact that an electron is lost with every ion. The quantity $k_L T$ is the mean energy lost per ion. If all of the particles are in the ideal regime, $k_L = 2.5$. In multiple mirrors, $k_L > 2.5$ due to the more rapid escape of ions in the low density regime. Ambipolar effects have

been accounted for in equation (12). Eliminating F_o between (19) and (12), we obtain

$$P_L = \frac{4k_L T v_{th} A_c n_c}{\sqrt{\pi} R_c \sigma_c} . \qquad (20)$$

We consider a non-ignited reactor with recirculating power P_R. The *power amplification factor* is defined as

$$Q = \frac{P_F}{P_R} . \qquad (21)$$

A large value of Q is desirable from an economic standpoint.

We rearrange the power balance equation and substitute from equations (15), (18), (20) and (21) to obtain

$$\frac{4k_L T v_{th} A_c n_c}{\sqrt{\pi} R_c \sigma_c} = \left[\left(\frac{1}{Q} + f_1 \right) \frac{W_F \langle \sigma v \rangle}{4} - k_\beta \sqrt{T} \right] M . \qquad (22)$$

Equation (22) can be manipulated[20] to form an expression for the product of the central cell pressure and the system length:

$$p_c L = X(T, k_L; N, Q, \beta, R_c, B_{vM}) . \qquad (23)$$

It is reasonable to assume that the cost of the system increases monotonically with $p_c L$.[14] We will therefore minimise it with respect to T and k_L. The quantities to the right of the semicolon in (23) are input parameters of the system. The optimum values of these parameters must be determined by an economic analysis which is beyond the scope of this study.[13] By fixing β, R_c, and B_{vM}, p_c is held constant, even if T varies. This insures that a minimum of $p_c L$ is a minimum of L.

Using equations (15), (22), and (16), an expression for the fusion power per unit central cell cross sectional area, P_F / A_c, can be obtained. There is

no way *within the model itself* to set upper and lower bounds on A_c. In Sec. V, independent criteria are found to set these bounds, but for now, A_c is a free parameter of the system. The quantity P_f/A_c tends to be too large for a practical power plant. We therefore try to minimize this, as well as $p_c L$. As an aside, we note that $p_c L$ does not depend on A_c.

III. RF Effects

We assume an ion cyclotron resonance field (ICRF) with its electric field vector perpendicular to the static magnetic field. An ICRF is applied to each cell on the side closest to the end of the system (see Fig. 4). We assume that $k_\perp r_L \ll 1$, and that $k_\parallel r_L \ll 1$, where r_L is the cyclotron radius. The frequency ω of the field is chosen equal to the ion cyclotron frequency Ω at some point in the mirror region. Centered about this *resonance point*, there is a *resonance zone* where $\Omega \approx \omega$. Because the mirror regions have large magnetic field gradients, the axial extent of a resonance zone is very small. We therefore treat any change in particle velocity due to the ICRF as an impulse in the perpendicular particle velocity delivered at the resonance point. An ion entering the resonance zone can gain or lose perpendicular energy depending on its gyrophase. On the average, energy is gained and the magnetic moment is increased.

The first order correction was calculated by Jaeger et al.[21] to be

$$v_{\perp 1} = \frac{2\pi eE}{m\omega} \left(\frac{2\omega L_r}{v_{\perp r}} \right)^{2/3} |\mathrm{Ai}(-z)| \cos \psi , \qquad (24)$$

where L_r is the magnetic field axial scale length at the resonance point, $\mathrm{Ai}(-z)$ is the airy function, ψ is the difference between the electric field phase and the

ion gyrophase, and $z = (2\omega L_r/v_{\perp r})^{2/3}(v_{sr}/v_{\perp r})^2$. The subscript "r" denotes a quantity evaluated at the resonance point. The phase difference ψ is considered to be randomized between resonance zone encounters by coulomb collisions in the cell midplane.[22] There are, therefore, no adiabatic barriers to heating.

A particle with pitch angle parameter $z = 0$ turns at the resonance point. As z increases, the turning point moves away from the resonance zone towards the mirror throat. Because

$$\left(\frac{2\omega L_r}{v_{\perp r}}\right)^{2/3} = \left(\frac{2L_r}{r_L}\right)^{2/3} \gg 1 ,$$

most particles that reach the resonance zone have $z \gg 1$.

We average over pitch angle in this limit, so the airy function can be replaced by its asymptotic, rms value. Equation (24) becomes

$$v_{\perp 1} = \frac{2eE}{m\omega}\left(\frac{\pi\omega L_r}{v_{sr}}\right)^{1/2} \cos\psi . \tag{25}$$

For the same limit, Rognlien and Matsuda[23] have calculated the phase averaged part of the second order change in the velocity,

$$\langle v_{\perp 2}\rangle = \frac{1}{v_{\perp r}}\left(\frac{eE}{m\omega}\right)^2\left(\frac{\pi\omega L_r}{v_{sr}}\right) . \tag{26}$$

There is also an oscillating part, $\tilde{v}_{\perp 2} = v_{\perp 2} - \langle v_{\perp 2}\rangle$.

We introduce energy-magnetic moment variables and define some dimensionless parameters. The velocities v_{sr} and $v_{\perp r}$ are transformed to Y and γ, where $Y = v/v_{th}$, and

$$\gamma = \frac{1}{\Omega(z)}\frac{v_\perp^2(z)}{v^2(z)} = \frac{1}{\Omega(z)}\sin^2\theta(z) ,$$

where $\theta(z)$ is the pitch angle. Y and γ are constants of the motion in the mirror region, except within resonance zone. The parameters are

$$\eta = \frac{\Omega_M}{\omega} ,$$

which marks the location of the resonance, and

$$\delta = \frac{eE}{m v_{th}} \left(\frac{\pi L_r}{\Omega_M v_{th}} \right)^{1/2} ,$$

a measure of the field strength. Here, Ω_M is the ion cyclotron frequency at the mirror throat. Note that $1 \leq \eta \leq R$, where R is the mirror ratio. Equation (25) becomes

$$v_{\perp 1} = 2 v_{th} \delta \sqrt{\eta/Y} \, (1 - \omega\gamma)^{-1/4} \cos\psi , \qquad (27)$$

and (26) becomes

$$\langle v_{\perp 2} \rangle = v_{th} \delta^2 \frac{\eta}{Y^2} \left[\omega\gamma(1 - \omega\gamma) \right]^{-1/2} . \qquad (28)$$

Pitch angle scattering arises from first order changes in $v_\perp$. We therefore discard the second order terms, and choose the rms value of $\cos\psi$ in (27) to obtain

$$v_o = v_{th} \delta \sqrt{2\eta/Y} \, (1 - \omega\gamma)^{-1/4} .$$

The midplane pitch angle is

$$\theta_o = \arcsin \sqrt{\Omega_o \gamma} .$$

Before the encounter with resonance, we have

$$\gamma = \frac{1}{\omega} \frac{v_{\perp r}^2}{v_{\perp r}^2 + v_{zr}^2} .$$

After the encounter, the new value of γ is

$$\bar{\gamma} = \frac{1}{\omega} \frac{(v_{\perp r} + v_o)^2}{(v_{\perp r} + v_o)^2 + v_{zr}^2} .$$

The average change in the midplane pitch angle during one bounce due to ICRF scattering is thus

$$\Theta_E(Y,\gamma) = \arcsin\sqrt{\Omega_o\bar{\gamma}} - \arcsin\sqrt{\Omega_o\gamma} \ . \tag{29}$$

The phase averaged energy absorbed by a single ion during a single pass through the resonance zone is

$$\langle\Delta W_{\perp r}\rangle = \frac{1}{2}m\left[2v_{\perp r}\langle v_{\perp 1}\rangle + \langle v_{\perp 2}\rangle + \bar{v}_{\perp 2}\rangle + \langle v_{\perp 1}^2\rangle\right] \ . \tag{30}$$

The terms $v_{\perp r}\langle v_{\perp 1}\rangle$ and $\langle \bar{v}_{\perp 2}\rangle$ average to zero. Thus, (30) becomes

$$\langle\Delta W_{\perp r}\rangle = \frac{2\pi L_r (eE)^2}{m\omega v_{sr}} \ . \tag{31}$$

Two classes of ions flow through the resonance in cell j: ions from cell j that can reach the resonance, and loss cone ions from cell $j-1$. The RF power absorbed in cell j is

$$P_j = n_j A_{rj} \int \langle\Delta W_{\perp r}\rangle v_{sr} f(\mathbf{v})\, d\mathbf{v}$$
$$+ n_{j-1} A_{rj} \int \langle\Delta W_{\perp r}\rangle v_{sr} f(\mathbf{v})\, d\mathbf{v} \ . \tag{32}$$

The first integral is taken over the velocity space of all ions in cell j that can reach the resonance point. The second integral is taken over the inward facing loss cone of cell $j-1$. The plasma cross sectional area at the resonance point is $A_{rj} = A_c\eta_j/R_c$. Noting that $\langle\Delta W_{\perp r}\rangle v_{sr}$ is independent of velocity, we obtain

$$P_j = mv_{th}^3 \frac{A_c\eta_j^2\delta_j^2}{R_c}\left[n_j\left(1-\sqrt{1-\eta_j/R_j}\right)\right.$$
$$\left.+ n_{j-1}\left(1-\sqrt{1-1/R_{j-1}}\right)\right] \ . \tag{33}$$

In an RF heated system, the recirculating power P_R is given by

$$P_R = 2\sum_{j=1}^{N} P_j \ .$$

This limits the amount of RF power that can be applied to the system. No RF is applied to the central cell because it is impossible to produce asymmetry there.

The asymmetry factor C_j is due to an RF induced change in the inward facing loss cone boundary in cell j. Without ICRH, the loss cone volume is given by

$$\gamma - \frac{1}{\Omega_M} \le 0 . \tag{34}$$

When ICRH is applied, γ changes to

$$\bar{\gamma} = \frac{1}{\omega} \frac{W_{\perp r} + \Delta W_{\perp r}}{W + \Delta W_{\perp r}} .$$

The new loss cone volume is thus

$$\gamma - \frac{1}{\Omega_M} + \left(\frac{1}{\omega} - \frac{1}{\Omega_M} \right) \frac{\Delta W_{\perp r}}{W} \le 0 . \tag{35}$$

Writing $\Delta W_{\perp r}$ in terms of the new variables, and clearing the denominators, (35) becomes

$$\begin{aligned}
&(\Omega_M \gamma - 1)(1 - \omega\gamma)^{1/2} Y^3 \\
&+ 4(\eta - 1)\sqrt{\Omega_M \gamma}(1 - \omega\gamma)^{1/4} Y^{3/2} \delta \cos\psi \\
&+ 4\eta(\eta - 1)\delta^2 \\
&+ 2\eta(\eta - 1)\delta^2 \cos 2\psi \\
&+ 2(\eta - 1)\sqrt{\omega\gamma}(1 - \omega\gamma)^{1/2} Y^3 \frac{\bar{v}_{\perp 2}}{v_{th}} \le 0
\end{aligned} \tag{36}$$

The loss cone edge for a given velocity class is found by integrating ψ and γ over that portion of velocity space where (36) is satisfied. In equation (36), the first term is zeroth order in δ, the second term is first order, and the third, fourth, and fifth terms are second order. Upon integration over ψ, the second, fourth and fifth terms, which are oscillatory in ψ, increase by an order.

One difficulty with (36) is that $\bar{v}_{\perp 2}$ was not evaluated. We have found numerically, however, that the loss cone boundary obtained by using the first three terms of (36) is virtually identical to that obtained by using the first four terms. Since the fourth term is of the same order as the fifth term, it follows that we can ignore the fifth term.

As it turns out, setting $\psi = \pi/2$ and $1 - \omega\gamma = 1$ in (36) produces a loss cone edge that closely approximates the numerically calculated edge (see Fig. 5). Then (36) becomes

$$\gamma - \frac{1}{\Omega_M}\left[1 - \frac{Y_{LC}^3}{Y^3}\right] \leq 0 , \tag{37}$$

where

$$Y_{LC}^3 = 2\eta(\eta - 1)\delta^2 . \tag{38}$$

Note that for $Y < Y_{LC}$, there is no loss cone.

Using (37) for the loss cone edge, we calculate the asymmetry factor. Combining (9) with the definitions of b_j^+ and b_j^-,

$$C_j = \frac{G_j}{F_{j-1}} \frac{\overline{F}_j}{\overline{G}_j} .$$

In the limit of zero net outward drift, $\overline{F}_j = \overline{G}_j$. G_j is given by (11). F_{j-1} is found by evaluating

$$F_{j-1} = A_j n_j \int v_z f(\mathbf{v}) \, d\mathbf{v}$$

over the loss cone volume given by (37). We obtain

$$C_j^{-1} = (Y_{LCj}^2 + 1)\exp(-Y_{LCj}^2) - \sqrt{\pi}\, Y_{LCj}^3\left[1 - \text{erf}(Y_{LCj})\right] . \tag{39}$$

Because of its position in the system, the central cell is always symmetric; $C_c = 1$.

We now choose the position of the resonance point (choose η_j) to maximise the asymmetry factor for fixed P_j. Since C_j is a monotonically increasing function of Y_{LCj}, we maximise Y_{LCj} with respect to η_j. Using the definition of Y_{LCj}, we substitute for δ_j^2 from (33). The term in (33) involving loss cone particles from cell $j - 1$ is independent of the resonance zone location in cell j, and is ignored. We obtain the function

$$g(\eta_j) = \frac{\eta_j - 1}{\eta_j} \left(1 - \sqrt{1 - \eta_j/R_j} \right)^{-1} \tag{40}$$

that must be maximised with respect to η_j. Setting the derivative equal to zero yields

$$\eta_j^3 - 6\eta_j^2 + (4R_j + 9)\eta_j - 8R_j = 0 . \tag{41}$$

For large values of R_j, $\eta_j \approx 2$. Even if R_j is as small as 3, $\eta_j = 1.75$. We therefore choose $\eta_j = 2$ for all j.

IV. Cell Lengths

The cell length l_j depends on the axial diffusion coefficients, the particle fluxes in the ideal and low density regimes, and the choice of *separation velocity* v_{sj} that separates the two regimes.

The ideal diffusion coefficient in cell j, D_{Ij}, is found by assuming that all of the particles are in the ideal regime. The diffusion equation then yields

$$F_o = -2A_j D_{Ij} \frac{dn}{dz} , \tag{42}$$

where the factor of 2 accounts for ambipolar effects. The axial density gradient is given by $-\Delta n_j/l_j$, where, from (12),

$$\Delta n_j = n_j - n_{j-1} = \frac{\sqrt{\pi}\, R_j}{v_{th} A_j} \left[1 + (1 - 1/C_j)\sigma_j \right] F_o .$$

Substituting this into (42) and solving for D_{Ij}, we obtain

$$D_{Ij} = \frac{v_{th} l_j}{2\sqrt{\pi} R_j} \left[1 + (1 - 1/C_j)\sigma_j\right]^{-1} .$$
(43)

In the symmetric case, this reduces to Makhijani's result,[7]

$$D_{Ij} = \frac{v_{th} l_j}{2\sqrt{\pi} R_j} .$$

Asymmetry is therefore seen to decrease the value of the diffusion coefficient .

The diffusion coefficient in the low density regime is found by using random walk theory. The calculation is carried out in appendix A, and yields

$$D_{Lj}(v) = \frac{v\lambda(v)}{4R_j} \left[1 - \frac{1}{C_j + 1} \frac{Y_{LCj}^3}{Y^3}\right]^2$$
$$\times \left[1 + \frac{\lambda(v)}{l_j}\Theta_{Ej}^2(v)\right]^{-1} \left[1 - (1 - 1/C_j)\sigma_j\right]^{-1} ,$$
(44)

where $Y = v/v_{th}$. When there is no ICRF, (44) reduces to the standard result,[7]

$$D_{Lj}(v) = \frac{v\lambda(v)}{4R_j^2} .$$

The net outward flux in cell j due to particles in the ideal regime is

$$F_{Ij} = \int F_{Ij}(v) \, dv .$$

For a particular velocity class,

$$F_{Ij}(v) \, dv = dv \, v^2 A_j n_j \int_0^{\pi} v \cos\theta f(v,\theta) \sin\theta \, d\theta .$$

The velocity distribution $f(v,\theta)$ is a drifting maxwellian. Here, the small drift term cannot be discarded as it is the term that produces the net flux. Evaluating the integral, we obtain

$$F_{Ij}(v) = \frac{8}{3\sqrt{\pi}} Y^4 \exp(-Y^2) A_j n_j v_{dj} ,$$
(45)

where v_{dj} is the drift velocity in cell j.

Analogously, in the low density regime, we find

$$F_{Lj}(v) = v^2 \int_0^\pi D_{Lj}(v)(-\nabla n)f(v,\theta)\sin\theta\,d\theta \tag{46}$$

$$= \frac{4}{\sqrt{\pi}} Y^2 \exp(-Y^2)D_{Lj}(v)(-\nabla n) .$$

The minimum net outward flux F_o occurs when all particles are in the ideal regime,

$$F_o = D_{Ij}(-\nabla n) = \int_0^\infty F_{Ij}(v)\,dv = A_j n_j v_{dj} . \tag{47}$$

Eliminating $A_j n_j v_{dj}$ between (45) and (47), we obtain,

$$F_I(v) = \frac{8}{3\sqrt{\pi}} Y^4 \exp(-Y^2)F_o . \tag{48}$$

The ideal flux is independent of the cell number, so the subscript "j" has been dropped in (48). Eliminating $(-\nabla n)$ between (46) and (47) gives

$$F_{Lj}(v) = \frac{4}{\sqrt{\pi}\,v_{th}} Y^2 \exp(-Y^2) \frac{D_{Lj}(v)}{D_{Ij}} F_o . \tag{49}$$

We choose the separation velocity in cell j to preserve continuity of flux:

$$F_I(v_{oj}) = F_{Lj}(v_{oj}) . \tag{50}$$

Inserting (48) and (49) into (50), we obtain

$$D_{Lj}(v_{oj}) = \frac{2}{3} Y_{oj}^2 D_{Ij} , \tag{51}$$

where $Y_{oj} = v_{oj}/v_{th}$. Using (43) and (44) in (51), and solving for the length of cell j, we get

$$l_j = \left\{ \frac{3\sqrt{\pi}}{4R_j Y_{oj}} \left[1 - \frac{1}{C_j+1} \frac{Y_{LOj}^3}{Y_{oj}^3} \right]^2 - \Theta_{Ej}^2(Y_{oj}) \right\} \lambda(Y_{oj}) . \tag{52}$$

In the absence of the ICRF, (52) reduces to

$$l_j = \frac{3\sqrt{\pi}}{4R_j Y_{oj}} \lambda(Y_{oj}) .$$

The separation velocity is determined from the axial power

$$P_L = 2A_j n_j \int \frac{1}{2} m v^2 v_z f(\mathbf{v}) \, d\mathbf{v} , \tag{53}$$

where the integral is taken over all of velocity space. The integral in (53) can be integrated over gyrophase and pitch angle, and split at the separation velocity. Since $m v^2/2 = TY^2$, we obtain

$$P_L = 2\left[\int_0^{v_{oj}} Y^2 \frac{F_I(v)}{F_o} \, dv + \int_{v_{oj}}^{\infty} Y^2 \frac{F_{Lj}(v)}{F_o} \, dv \right] T F_o . \tag{54}$$

The term in brackets is the axial power loss correction factor k_L.

Substituting (48) and (49) into (54), we obtain

$$k_L = \int_0^{Y_{oj}} \frac{8}{3\sqrt{\pi}} Y^6 \exp(-Y^2) \, dY + \int_{Y_{oj}}^{\infty} \frac{4}{\sqrt{\pi}} Y^4 \exp(-Y^2) \frac{D_{Lj}(Y)}{D_{Ij}} \, dY . \tag{55}$$

Since k_L is constant thoughout the system, but D_{Lj} is not, v_{oj} varies from cell to cell. Given k_L, equation (55) can be solved numerically for v_{oj}. When performing the numerical calculations in the next section to minimize $p_o L$, trial values of T and k_L are chosen. These are used to find the v_o's, which, in turn, are used to find the cell lengths.

V.   Numerical Results

In this section, we present numerical solutions of the power balance equations, showing the variation of the system length L and the fusion power density P_F/A_c with respect to the input parameters. Reference design values for some of the input parameters are chosen. We then estimate the radial diffusion due to ICRH and that due to coulomb collisions, which yields a lower bound on the central cell plasma cross sectional area A_c. Finally, we compare our reactor results to those of previous studies.

Since the multiple mirror is a collisional device, we expect L to scale as the mean free path λ^*. When β and R_c are held constant, $\lambda^* \sim 1/n$ and $n \sim B_{vM}{}^2$. The fusion power density should be proportional to Ln^2. All numerical solutions for systems with or without ICRF show

$$L \sim B_{vM}{}^{-2} , \qquad \frac{P_F}{A_c} \sim B_{vM}{}^2 ,$$

confirming the scaling arguments.

System length and fusion power density are found to be sensitive functions of midplane β. With constant B_{vM} and R_c, density increases with increasing β. L should therefore decrease, while P_F/A_c should increase as β increases in value. Systems with and without ICRF are found to scale identically with β. Thus, in Fig. 6, only the curves for the system without the ICRF are shown. Efficient use of the field demands a high value of β. In order to easily compare our results with those of earlier studies,[6,14] we choose $\beta = 0.8$.

When R_c is varied while holding B_{vM} and β constant, $\lambda^* \sim 1/nR_c$. From (1), $nR_c^2 \approx \text{const}$, and we have $L \sim R_c$. This scaling is borne out by the numerical results for systems with no ICRF. The addition of ICRF changes the numerically determined scaling to $L \sim R_c^{1/2}$. A simple scaling argument for the fusion power density yields

$$\frac{P_F}{A_c} \sim Ln^2 \sim LR_c^{-4} .$$

This scaling is approximately supported by the numerical results, which indicate that $P_F/A_c \sim R_c^{-2.8}$ with or without ICRF. We choose Najmabadi's value:[14] $R_c = 3.363$. This value of the mirror ratio keeps the system length reasonably short.

The numerical results show that both L and P_F/A_c are monotonically increasing functions of Q (see Figs. 7 and 8). At ignition, $(Q = \infty)$ a 21 cell reactor with $B_{vM} = 240$ kG is approximately 2 km long and produces 3 Gwatts/cm^2 of fusion power. For finite values of Q, the addition of the ICRF shortens the system length and decreases P_F/A_c. We will choose a value of Q large enough to be economically interesting, but small enough to keep L and P_F/A_c at reasonable levels: $Q = 5$.

System length and fusion power density are found to be decreasing functions of N (see Figs. 9 and 10). Economic studies show[13] that the optimum number of cells $(2N + 1)$ for a multiple mirror system lies between 21 and 41. The high magnetic fields needed by mirrors are expensive to produce. Since the curves in Fig. 9 flatten out as N gets large, there is not much to be gained by having more than 41 cells.

The addition of the ICRF leads to enhanced pitch angle scattering and loss cone plugging. The loss cone plugging may be concentrated at one end (asymmetric), or split evenly between two resonance zones in the cell (symmetric). The relative importances of ICRF induced scattering and asymmetry are shown in Fig. 11. Asymmetrically applied ICRF can shorten a 21 cell system by 27 percent, and shorten a 41 cell system by 21 percent (curve "c" Fig. 11). If the ICRF power is applied in a symmetric fashion (two equal heating zones in each cell), the system length is reduced by less than 5 percent (curve "a" Fig. 11). If we set $\Theta_{Ej}^2 = 0$ in (44) and (52), the effects of ICRF induced pitch angle scattering are eliminated from the calculation. Without this scattering, we have curve "b", the system length reduction due to asymmetry alone. Comparing

curves "b" and "c", it can be seen that ICRF scattering accounts for only 2 percent of the system length reduction.

So far, the recirculating power has been divided equally among the cells. We have studied the effect of varying this distribution, seeking a minimum in L. The fraction of recirculating power in cell j is chosen to be

$$\alpha_j = \frac{h^N(h-1)}{h^j(h^N-1)} \,,$$

where $h > 1$. This weights the distribution towards the end cells. An optimum is found at $h \approx 1.5$ for both 21 and 41 cell systems (see Fig. 12). The improvement in length is approximately 8 percent when compared to the "flat" input distribution. All of the scaling laws presented earlier in this section are still valid.

Up to this point, radial diffusion has been ignored. Given a radial density profile, however, ions will be lost by radial diffusion. The radial confinement time can be written

$$T_r = \left(\frac{r_p}{l_r}\right)^2 \tau \,,$$

where r_p is the radius of the plasma column, l_r is the radial step length, and τ is the radial step time. There are two scattering processes that can cause radial diffusion: ICRH and coulomb collisions.

Consider self collisions among hydrogen isotope ions. This gives rise to like particle diffusion, which, to lowest order, results in no net radial diffusion. Tussewski and Lichtenberg[24] found a higher order correction which gives a radial confinement time of

$$T_{ri} = \frac{8\pi}{12}\left(\frac{r_p}{r_L}\right)^4 \tau_{ii} \,,$$

where τ_{ii} is the ion-ion $90°$ scattering time and the step length is an ion gyro-radius. When ions collide with electrons, ambipolar diffusion results. For this process, we estimate a radial confinement time of

$$T_{re} = \left(\frac{m_i}{m_e}\right)^{1/2} \left(\frac{r_p}{r_L}\right)^2 \tau_{ii} .$$

Typically, $r_p/r_L \approx 10$, therefore $T_{ri} \approx 5 T_{re}$. The radial diffusion rate due to ICRF is calculated using single particle theory in appendix B. We find that it is much slower than the diffusion rate due to coulomb collisions. Hence, the radial confinement time is determined by the ambipolar diffusion rate.

Another way to enhance coulomb scattering and shorten the system length is to add high Z impurities to the plasma.[11] We have the effect of these impurities on radial loss. The radial confinement time is given by

$$T_{rI} = \frac{n_i}{Z^2 n_I} \left(\frac{r_p}{r_L}\right)^2 \tau_{ii} ,$$

where n_I is the impurity density. An optimum Z and n_I $(n_i/Z^2 n_I \approx 3)$ can decrease L by about 25 percent.[20] However,

$$T_{rI} \approx .03 T_{re} .$$

The inclusion of high Z impurities increases the radial loss rate by an order of magnitude. This leads to unacceptably large fusion power output in a steady state reactor.

The value of T_r changes from cell to cell. Defining ν_j as the radial loss rate in cell j, the average radial loss rate is

$$\frac{1}{\overline{T}_r} = \frac{\nu_c n_c l_c + 2 \sum_{j=1}^{N} \nu_j n_j l_j}{n_c l_c + 2 \sum_{j=1}^{N} n_j l_j} .$$

In order that our one dimensional model be reasonably accurate, the radial confinement time must be large compared to the axial confinement time:

$$T_L = \frac{1}{2F_o} \left[A_c l_c n_c + 2 \sum_{j=1}^{N} A_j l_j n_j \right] .$$

Tussewski and Lieberman[12] made a detailed study of this problem, and concluded that if $T_r \geq 4T_L$, radial loss will reduce the particle confinement time by less than 10 percent. We use this criterion to determine the minimum value of A_c:

$$A_c = 4T_L \left(\frac{A_c}{T_r} \right) ,$$

where A_c/T_r is independent of A_c. Multiplying P_F/A_c by this value of A_c, and correcting for the radial density profile ($\bar{n}^2 \approx 0.5n^2$) yields the fusion power generated.

In 1974, Logan et al.[6] made a multiple mirror reactor calculation assuming 20 five meter cells on either side of a central solenoid. The average β was 0.8, and the peak field was 300 kG. By choosing the cells to be uniform in length, Logan et al. ignored the fact that the mean free path changes throughout the system. This results in an underestimation of the power lost out of the ends, and therefore, an underestimate of the system length. By varying the length of the central cell, Q could be changed. The length of a self sustaining reactor ($Q = \infty$) was calculated to be 1100 meters. The minimum Q for an economically viable reactor was judged to be 3. In this case, the length was estimated at 400 meters. Note that that the central cell comprises at least half of the system length in these designs.

Najmabadi et al.[14] made a more careful calculation assuming 20 cells of varying length on each side of a central solenoid. The plasma remains in the

intermediate mean free path regime throughout the system. The midplane β is 0.8 in each cell, and the peak field is 280 kG. With a Q of 5, the system length is 770 meters, where an optimisation over the temperature was performed. The central cell accounts for half of this length.

We made a reactor calculation using Najmabadi's input parameters, optimising over k_L as well as temperature. Without the ICRF, the system length is 750 meters, which agrees well with previous results. The addition of the ICRF reduces L to 530 meters, an improvement of 30 percent. The fusion power produced by this system is 8.6 GW.

Because ICRH is more efficient in a system with fewer cells (see Fig. 11), we favor a 21 cell machine. With $B_{vM} = 280$ kG, $L = 580$ meters and $P_f = 6.3$ Gwatts. Thus, we can eliminate half of the mirror coils at the cost of 50 meters of length. In the event that a peak field of 280 kG is too large to be practical, the field can be lowered for an increase in length, with the scaling $L \sim B_{vM}^{-2}$. Four detailed reactor designs with $B_{vM} = 240$ kG are presented in appendix C. A 21 cell system is then 790 meters long.

In conclusion, we have shown that asymmetrically applied ICRH can significantly reduce the system length in a multiple mirror cell reactor. A 21 cell reactor with a peak field of 280 kG and $Q = 5$ is reduced from 845 meters to 580 meters in length, an improvement of 30 percent. The fusion power produced by the system is approximately 6300 MW, a reasonable amount for a practical power plant.

Acknowledgments

Appendix A: The Low Density Diffusion Coefficient

A particle in the low density regime will be trapped in a single cell for an average time $\tau_t(v)$. When scattered into the loss cone, it will travel an average distance $l_s(v)$ before being retrapped in an average time $\tau_f(v)$. In a system with large mirror ratios, $\tau_t(v) \gg \tau_f(v)$ and $l_s(v) \approx v\tau_f(v)$. The diffusion coefficient is

$$D(v) = \frac{l_s^2(v)}{2[\tau_t(v) + \tau_f(v)]} \approx \frac{l_s^2(v)}{2\tau_t(v)} . \tag{A1}$$

For an isotropic distribution (with large mirror ratios), the ratio of free time to trapped time is

$$\frac{\tau_f(v)}{\tau_t(v)} = \frac{1}{2} \sin^2 \theta_{LC}(v) . \tag{A2}$$

Loss cone asymmetry reduces $\tau_f^+(v)$ by shrinking the outward facing loss cone. (A "+" superscript denotes the direction away from the center, while a "-" superscript denotes the opposite.) The outward step length is therefore shorter than the inward step length. This *asymmetric random walk* process produces an inward drift

$$
\begin{aligned}
B(v) &= \frac{b_j^-}{b_j^- + b_j^+} \frac{v\tau_f^-(v)}{\tau_t(v)} - \frac{b_j^+}{b_j^- + b_j^+} \frac{v\tau_f^+(v)}{\tau_t(v)} \\
&= \frac{v}{2} \frac{C_j \sin^2 \theta_{LC}^-(v) - \sin^2 \theta_{LC}^+(v)}{C_j + 1} ,
\end{aligned}
\tag{A3}
$$

where we have used the definition of C_j and (A2). To evaluate (A1), we find the average step length $\bar{l}_s(v) = (l_s^+(v) + l_s^-(v))/2$. Using the definition of $l_s(v)$, the definition of C_j, and (A2), the diffusion coefficient becomes

$$D(v) = \frac{v^2}{4} \left[\frac{C_j \sin^2 \theta_{LC}^-(v) + \sin^2 \theta_{LC}^+(v)}{C_j + 1} \right] \left[\frac{C_j \tau_f^-(v) + \tau_f^+(v)}{C_j + 1} \right] . \tag{A4}$$

The mean free time $\tau_f(v)$ is the time for an ion to scatter through a loss cone angle. There are two independent scattering mechanisms: ICRH and coulomb collisions. For coulomb collisions, the mean free time is

$$\tau_c(v) = \frac{\lambda(v)}{v} \sin^2 \theta_{LC}(v) ,$$

while for the ICRH, we have

$$\tau_E(v,\theta) = \frac{l_j}{v_s} \frac{\sin^2 \theta_{LC}(v)}{\Theta_E^2(v,\theta)} ,$$

where Θ_E is given by equation (29). We eliminate the pitch angle dependence of τ_E by choosing $\sin^2 \theta = 1/R_j$ and replacing v_s by v in τ_E. The mean free time is thus

$$\tau_f(v) = \frac{\lambda(v)}{v} \left[1 + \frac{\lambda(v)}{l_j} \Theta_E^2(v) \right]^{-1} \sin^2 \theta_{LC}(v) . \tag{A5}$$

The loss cone edges are given by

$$\sin^2 \theta_{LC}^-(v) = \frac{1}{R} , \qquad \sin^2 \theta_{LC}^+(v) = \frac{1}{R} \left(1 - \frac{Y_{LC}^3}{Y^3} \right) , \tag{A6}$$

where $Y = v/v_{tA}$ and Y_{LC} is defined by (38). The drift and the diffusion (equations (A3) and (A4)) can now be completely evaluated.

The low density diffusion coefficient must satisfy an equation similar to (42). To this end, we use $B(v)$ and $D(v)$ obtained above to determine $n(s)$ the axial density profile of ions in the low density regime. This $n(s)$ is then used to find $D_L(v)$, the low density diffusion coefficient .

Combining the continuity equation and the momentum equation, we have

$$D(v)\frac{\partial^2 n}{\partial s^2} + B(v)\frac{\partial n}{\partial s} = 0 \tag{A7}$$

in the steady state, where we have assumed that $D(v)$ and $B(v)$ are weak functions of s over the length of the system L. With the center of the system at

$s = 0$, we have the boundary condition $n(L/2) = 0$. Solving (A7) and applying the boundary condition yields

$$n(s,v) = \frac{\Gamma}{B(v)} \left\{ \exp\left[\frac{B(v)}{D(v)} \left(\frac{L}{2} - s \right) \right] - 1 \right\}, \qquad \text{(A8)}$$

where Γ is the net outward ion flux. We now find $D_L(v,s)$ from

$$\Gamma = -D_L(v,s)\frac{\partial n}{\partial s} .$$

Substituting for $n(s,v)$ from (A8), we obtain

$$D_L(v,s) = D(v)\exp\left[-\frac{B(v)}{D(v)} \left(\frac{L}{2} - s \right) \right]. \qquad \text{(A9)}$$

If we assume that asymmetry causes the same exponential dependence in the low density regime as in the ideal regime, we have

$$\exp\left[-\frac{B(v)}{D(v)} \left(\frac{L}{2} - s \right) \right] \approx \left[1 + (1 - 1/C_j)\sigma_j \right]^{-1}.$$

The low density diffusion coefficient in cell j can then be written

$$D_{Lj}(v) = \frac{v\lambda(v)}{4} \left[\frac{C_j \sin^2\theta_{LC}^-(v) + \sin^2\theta_{LC}^+(v)}{C_j + 1} \right]^2$$
$$\times \left[1 + \frac{\lambda(v)}{l_j}\Theta_{Ej}^2(v) \right]^{-1} \left[1 + (1 - 1/C_j)\sigma_j \right]^{-1}.$$

Using equations (A6) yields (44) in section IV.

Appendix B: Radial Diffusion due to ICRH

The passage of an ion through the resonance zone will change its guiding center radius. To compute this change, we model the resonance zone as a uniform B field in the s direction and a resonant E field. This E field rotates in the x-y plane and is a function of s only, being nonzero only in the space

between $s = 0$ and $s = L_r$. We assume that an ion spends many gyroperiods in the resonance zone.

The equations of motion are

$$\frac{dv_x}{dt} = \Omega v_y + \frac{e}{m} E_x ,$$

$$\frac{dv_y}{dt} = -\Omega v_x + \frac{e}{m} E_y ,$$

$$\frac{dv_z}{dt} = 0 ,$$

where

$$E_x = -E(s) \sin \Omega t ,$$

and

$$E_y = -E(s) \cos \Omega t .$$

In a uniform field, the guiding center coordinates are given by

$$X_g = x + \frac{v_y}{\Omega} ,$$

$$Y_g = y - \frac{v_x}{\Omega} ,$$

$$Z_g = z .$$

Taking the time derivatives of the guiding center equations, we substitute from the equations of motion and form the complex quantity $\Delta R_g = X_g - iY_g$. We then obtain

$$\frac{dR_g}{dt} = -\frac{e}{m\Omega} E(s) \exp(i\Omega t) . \tag{B1}$$

To find the change in R_g, we integrate (B1) from $s = 0$ to $s = L_r$:

$$\Delta R_g = -\frac{e}{m\Omega} \int E(s) \exp(i\Omega t) \, dt . \tag{B2}$$

Time is related to s by $s = v_z t$ where v_z is constant.

We will find the general solution to (B2) if $E(s)$ and Ξ its first two derivatives are continuous for all s. The fact that the ion spends many gyroperiods in the resonance zone permits an asymptotic solution to (B2). We deform the contour of integration into the complex plane as shown in Fig. 12. Writing $s = \alpha + i\beta$, (B2) becomes

$$\Delta R_g = -\frac{ie}{m\Omega} \int_0^\infty E(s) \exp\left(-\frac{\Omega\beta}{v_s}\right) d\beta \\ + \frac{ie}{m\Omega} \int_0^\infty E(s) \exp\left(-\frac{\Omega\beta}{v_s} + i\frac{\Omega L_r}{v_s}\right) d\beta , \tag{B3}$$

where the integrals are over C_1 and C_3, respectively. The integral over C_2 does not contribute to ΔR_g. Because of the exponential, the dominant contribution to (B3) will come from the parts of the contour near the real axis. We therefore expand $E(s)$ in a Taylor series about the points where $\beta = 0$,

$$E(s) = -\frac{1}{2}E''\beta^2 + \ldots$$

("$''$" denotes differentiation with respect to s). The first two terms of the Taylor series vanish due to the continuity condition on $E(s)$. Integrating (B3), we obtain

$$\Delta R_g = \frac{iev_s^2}{m\Omega^4} \left[E''(0) - E''(L_r) \exp\left(i\frac{\Omega L_r}{v_s}\right) \right] .$$

Multiplying by the complex conjugate and taking the square root,

$$|\Delta R_g| = \frac{ev_s^2}{m\Omega^4} \left[E''^2(0) + E''^2(L_r) - 2E''(0)E''(L_r) \cos\left(\frac{\Omega L_r}{v_s}\right) \right]^{1/2} . \tag{B4}$$

We assume that

$$E''(0) \approx E''(L_r) \approx \frac{\overline{E}}{L_r^2} ,$$

where $\overline{E}$ is the average value of the electric field. The cosine term in (B4) is gyrophase dependent and will be discarded. Approximating v_s by v_{tA}, (B4)

becomes

$$|\Delta R_g| = \left[\frac{e\overline{E}L_r}{mv_{th}^2}\right]\left(\frac{r_L}{L_r}\right)^3 r_L .$$ (B5)

The term in square brackets is the ratio of electric field energy to thermal energy, which is usually much less than unity. The ratio r_L/L_r is typically 10^{-2}. This makes the radial step length much shorter than that due to coulomb collisions. The radial step time $\tau_E(v)$, calculated in appendix A, has been shown numerically to be much longer than $\tau_c(v)$, its coulomb counterpart. Therefore, the radial diffusion rate due to ICRH is much less than that due to coulomb collisions.

Appendix C: Reactor Designs

All of the designs in this appendix have $Q = 5$, $R_c = 3.363$, $B_{vM} = 240$ kG, $\beta = 0.8$ and a vacuum magnetic field strength of 137 kG in the central cell. In these tables, n is the hydrogen ion density, given in units of 10^{15} cm^{-3}, l is the cell length, in meters, and R is the finite β mirror ratio. For the examples with ICRF, the column labeled "RF" is the percentage of RF power injected into the cell, E is the magnitude of the electric field, in kV/cm^2, and C is the asymmetry factor. The components of the power flow are: the total fusion power P_F, the axial power loss P_L, and the bremsstrahlung power loss P_β. central cell cross sectional area basis.

The numbers are given to three or more places in some cases. However, the accuracy of the model is only to within 10 percent, so only two figures are significant. Note that the cell number increases as one moves towards the center of the system (cell 1 is the end cell).

Design 1: 21 cells, no ICRF

$T = 6.37 \ keV$

$\tau_{mm} = 44.7 \ msec$

$p_oL = 6.90 \cdot 10^{10} \ joules/m^2$

$L = 1152 \ meters$

$h_L = 3.19$

$Y_o = 1.92$

$P_F/A_c = 1.34 \ gigawatts/cm^2$

$P_L/A_c = .406 \ gigawatts/cm^2$

$P_\beta/A_c = .088 \ gigawatts/cm^2$

$n_c = 2.94 \cdot 10^{16} \ cm^{-3}$

$l_c = 556 \ meters$

$A_c = 6.0 \ cm^2$

cell	n	l	R
1	2.67	54.6	12.82
2	5.34	39.9	8.96
3	8.01	33.3	7.22
4	10.70	29.5	6.17
5	13.40	26.9	5.45
6	16.00	25.0	4.91
7	18.70	23.6	4.48
8	21.40	22.5	4.13
9	24.00	21.6	3.84
10	26.70	20.9	3.58

Design 2: 41 cells, no ICRF

$T = 5.42 \; keV$

$\tau_{mm} = 77.5 \; msec$

$p_oL = 6.09 \cdot 10^{10} \; joules/m^2$

$L = 1017 \; meters$

$h_L = 3.70$

$Y_o = 1.75$

$P_F/A_c = .866 \; gigawatts/cm^2$

$P_L/A_c = .228 \; gigawatts/cm^2$

$P_\beta/A_c = .090 \; gigawatts/cm^2$

$n_c = 3.45 \cdot 10^{16} \; cm^{-3}$

$l_c = 412 \; meters$

$A_c = 12.7 \; cm^2$

cell	n	l	R
1	1.64	36.0	17.82
2	3.29	26.1	12.52
3	4.93	21.7	10.16
4	6.58	19.1	8.74
5	8.22	17.3	7.77
6	9.86	16.0	7.04
7	11.50	15.0	6.48
8	13.20	14.2	6.02
9	14.80	13.5	5.63
10	16.40	12.9	5.31
11	18.10	12.4	5.02
12	19.70	12.0	4.77
13	21.40	11.7	4.55
14	23.00	11.4	4.35
15	24.70	11.1	4.18
16	26.30	10.8	4.01
17	27.90	10.6	3.86
18	29.60	10.4	3.72
19	31.20	10.2	3.59
20	32.90	10.1	3.47

Design 3: 21 cells, ICRF

$T = 6.43\ keV$

$\tau_{mm} = 48.1$ msec

$p_o L = 4.72 \cdot 10^{10}$ joules/m^2

$L = 788$ meters

$k_L = 3.54$

$1.87 \geq Y_o \geq 1.84$

$P_F/A_c = 1.00$ gigawatts/cm^2

$P_L/A_c = .304$ gigawatts/cm^2

$P_\beta/A_c = .064$ gigawatts/cm^2

$n_o = 2.91 \cdot 10^{16}$ cm^{-3}

$l_o = 338$ meters

$A_c = 6.3$ cm^2

cell	n	l	R	RF	E	C
1	4.93	31.2	9.30	33.9	3.44	2.778
2	9.05	26.9	6.73	22.6	1.58	1.353
3	12.30	24.4	5.67	15.1	0.96	1.140
4	15.10	22.7	5.05	10.1	0.64	1.069
5	17.50	21.5	4.64	6.7	0.46	1.036
6	19.60	20.8	4.32	4.5	0.34	1.021
7	21.70	20.0	4.07	3.0	0.25	1.013
8	23.60	19.4	3.86	2.0	0.19	1.007
9	25.50	19.0	3.67	1.3	0.14	1.005
10	27.40	18.8	3.51	0.9	0.11	1.003

Design 4: 41 cells, ICRF

$T = 5.53 \; keV$

$r_{mm} = 81.7 \; msec$

$p_oL = 4.31 \cdot 10^{10} \; joules/m^2$

$L = 720 \; meters$

$k_L = 4.10$

$1.75 \geq Y_o \geq 1.71$

$P_F/A_o = .678 \; gigawatts/cm^2$

$P_L/A_o = .183 \; gigawatts/cm^2$

$P_\beta/A_o = .067 \; gigawatts/cm^2$

$n_c = 3.38 \cdot 10^{16} \; cm^{-3}$

$l_o = 228 \; meters$

$A_o = 12.7 \; cm^2$

cell	n	l	R	RF	E	C
1	3.72	19.6	11.62	28.6	3.38	3.229
2	7.01	16.7	8.36	20.4	1.60	1.438
3	9.66	15.4	7.04	14.6	0.99	1.183
4	11.80	14.2	6.31	10.4	0.70	1.095
5	13.70	13.4	5.81	7.4	0.52	1.056
6	15.40	12.9	5.45	5.3	0.39	1.034
7	16.90	12.4	5.17	3.8	0.31	1.021
8	18.20	12.3	4.94	2.7	0.24	1.013
9	19.60	11.7	4.74	1.9	0.19	1.009
10	20.80	11.5	4.57	1.4	0.15	1.005
11	22.00	11.4	4.42	1.0	0.12	1.003
12	23.30	11.0	4.27	0.7	0.10	1.003
13	24.40	11.0	4.15	0.5	0.08	1.001
14	25.60	10.7	4.03	0.4	0.06	1.001
15	26.80	10.7	3.92	0.3	0.05	1.001
16	28.00	10.5	3.81	0.2	0.04	1.001
17	29.20	10.3	3.71	0.1	0.03	1.001
18	30.30	10.1	3.62	0.1	0.03	1.001
19	31.50	10.1	3.53	0.1	0.02	1.001
20	32.70	10.0	3.44	0.0	0.02	1.001

References

[1] R. F. Post, *Phys. Rev. Lett.* **18** 232 (1967)

[2] B. G. Logan, A. J. Lichtenberg, M. A. Lieberman and A. Makhijani, *Phys. Rev. Lett.* **28** 144 (1972)

[3] R. Bravenec, A. J. Lichtenberg, M. A. Lieberman and H. L. Berk, *Phys. Fluids* **24** 1320 (1982)

[4] G. Budker, V. Mirnov and D. Ryutov, *Zhetf Pis. Red.* **14** 320 (1971) [*JETP Lett.* **14** 212 (1971)]

[5] V. V. Mirnov and D. D. Ryutov, *Nuclear Fusion* **12** 627 (1972)

[6] B. G. Logan, I. G. Brown, A. J. Lichtenberg and M. A. Lieberman, *Phys. Fluids* **17** 1302 (1974)

[7] A. Makhijani, A. J. Lichtenberg, M. A. Lieberman and B. G. Logan, *Phys. Fluids* **17** 1291 (1974)

[8] J. Riordan, M. Tuszewski and A. J. Lichtenberg, *Plasma Physics* **20** 139 (1978)

[9] J. Riordan, A. J. Lichtenberg and M. A. Lieberman, *Nuclear Fusion* **19** 21 (1978)

[10] M. Tuszewski, D. Price, M. A. Liberman, R. Bravenec, K. Doniger, C. Hartman and A. J. Lichtenberg, *Nuclear Fusion* **19** 1244 (1979)

[11] S. Yang and M. A. Lieberman, *Nuclear Fusion* **17** 697 (1977)

[12] M. Tuszewski and M. A. Lieberman, *Phys. Fluids* **24** 320 (1981)

[13]F. Najmabadi, A. J. Lichtenberg and M. A. Lieberman, *Engineering Problems of Fusion Research, Proc. 8th Symp. San Francisco, California Nov. 1979 IEEE vol2 632* (1979)

[14]F. Najmabadi, A. J. Lichtenberg and M. A. Lieberman, *Nucl. Fusion 23 600* (1983)

[15]R. F. Post and X. Z. Li, *Nuclear Fusion 21 135* (1981)

[16]M. Hayes and J. S. DeGroot, *Phys. Lett. 86A 161* (1981)

[17]H. Price, N. Benjamin, B. Kang, M. A. Lieberman and A. J. Lichtenberg, to be published in *Phys. Fluids*

[18]G. Schmidt, *"Physics of High Temperature Plasmas."* Academic Press, New York, 1979.

[19]F. Najmabadi, A. J. Lichtenberg and M. A. Lieberman, *Phys. Fluids 26 1018* (1983)

[20]K. J. Doniger, *Ph.D Thesis, Department of Electrical Engineering and Computer Science, University of California at Berkeley* (1983)

[21]F. Jaeger, A. J. Lichtenberg and M. A. Lieberman, *Plasma Physics 14 1073* (1972)

[22]H. Momota and T. Takisuka, *Physics of Fluids 17 2290* (1974)

[23]T. Rognlien and Y. Matsuda, *Nuclear Fusion 21 345* (1981)

[24]M. Tussewski and A. J. Lichtenberg, *Phys. Fluids 20 1263* (1977)

Definitions

Sections

I	\frst
II	\scnd
III	\thrd
IV	\frth
V	\ffth

Appendices

A	\appa
B	\appb
C	\appc

References

1	\postI
2	\loganI
3	\brav
4	\budker
5	\mirnov
6	\loganII
7	\makh
8	\riordI
9	\riordII
10	\tusaII
11	\yang
12	\tusa
13	\najm
14	\najmI
15	\post
16	\hayes
17	\price
18	\schmidt
19	\najmII
20	\don
21	\jaeger
22	\momota
23	\rogn
24	\tusI

Equations

1	\bnum
2	\cnum
3	\dnum
4	\fnum
5	\gnum
6	\hnum
7	\jnum
8	\knum
9	\lnum
10	\mnum
11	\nnum
12	\pnum
13	\qnum
14	\rnum
15	\snum
16	\tnum
17	\vnum
18	\wnum
19	\xnum
20	\ynum
21	\snum
22	\bbnum
23	\ccnum
24	\ddnum
25	\ffnum

26	\ggnum
27	\hhnum
28	\jjnum
29	\kknum
30	\llnum
31	\mmnum
32	\nnnum
33	\ppnum
34	\qqnum
35	\ssnum
36	\ttnum
37	\vvnum
38	\wwnum
39	\xxnum
40	\yynum
41	\aanum
42	\bcnum
43	\cdnum
44	\dfnum
45	\fgnum
46	\ghnum
47	\hjnum
48	\jknum
49	\klnum
50	\lmnum
51	\mnnum
52	\npnum
53	\pqnum
54	\qrnum
55	\rsnum
A1	\cbnum
A2	\dcnum
A3	\fdnum
A4	\gfnum
A5	\hgnum
A6	\jhnum
A7	\kjnum
A8	\lknum
A9	\mlnum
B1	\bdnum
B2	\bfnum
B3	\bgnum
B4	\bhnum
B5	\bjnum
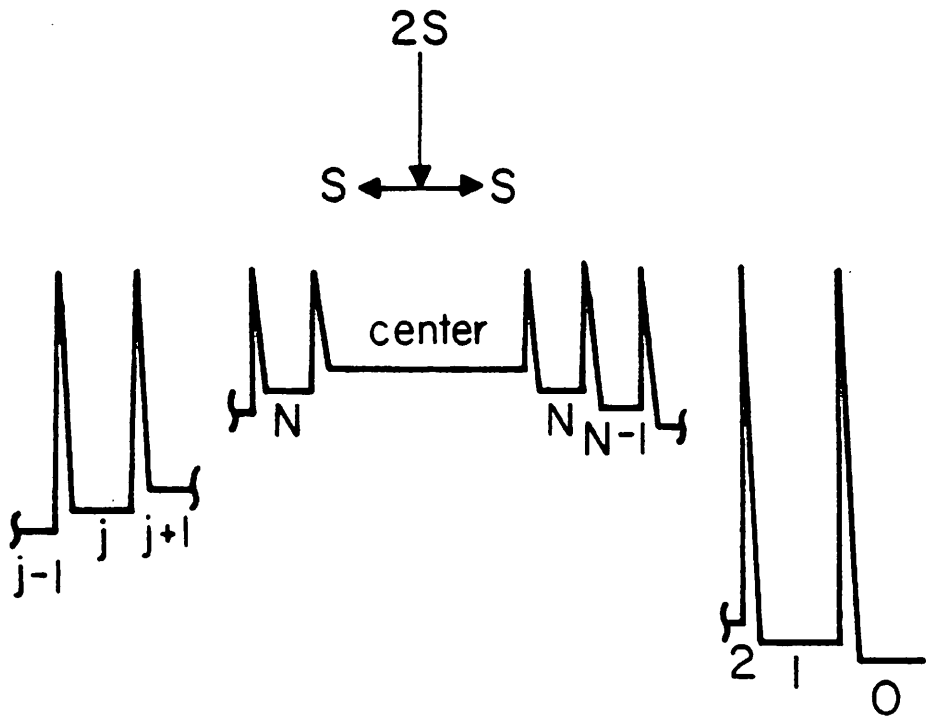
Fig. 1. The magnitude of the vacuum magnetic field versus z. Note the cell numbering. There is a plasma source of strength 2S in the center of the system.
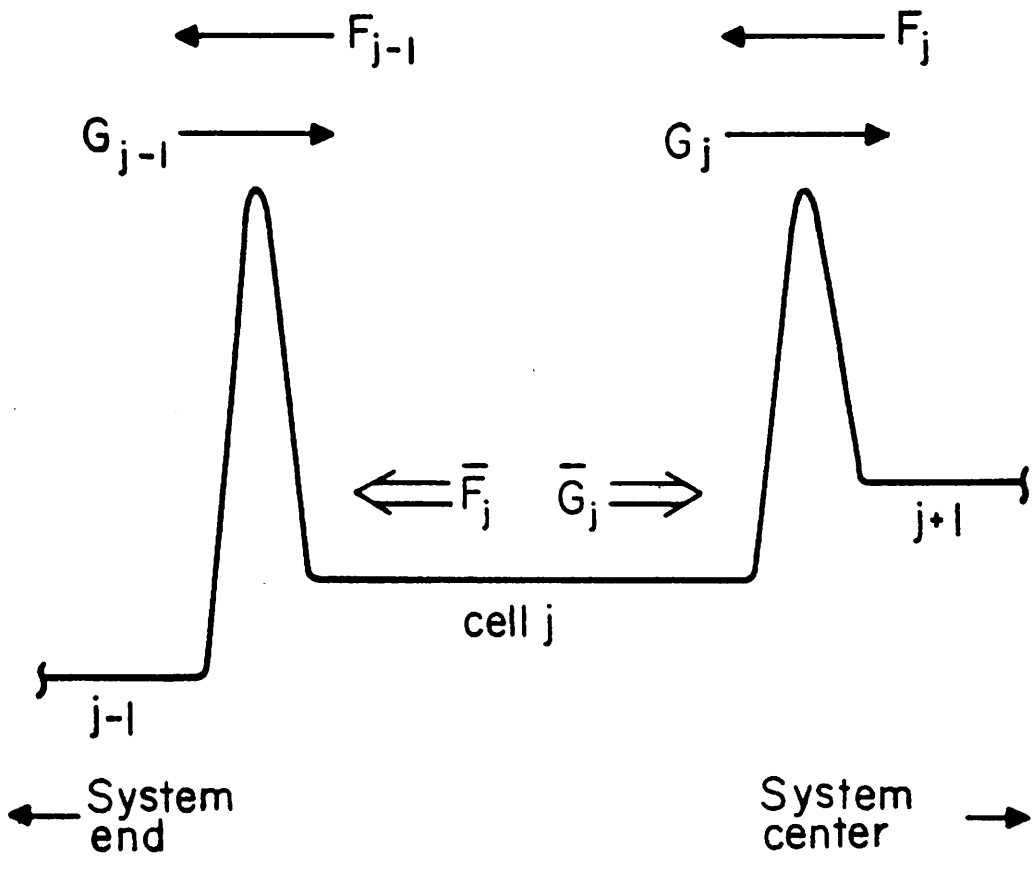
Fig. 2. Various particle fluxes affecting cell j.
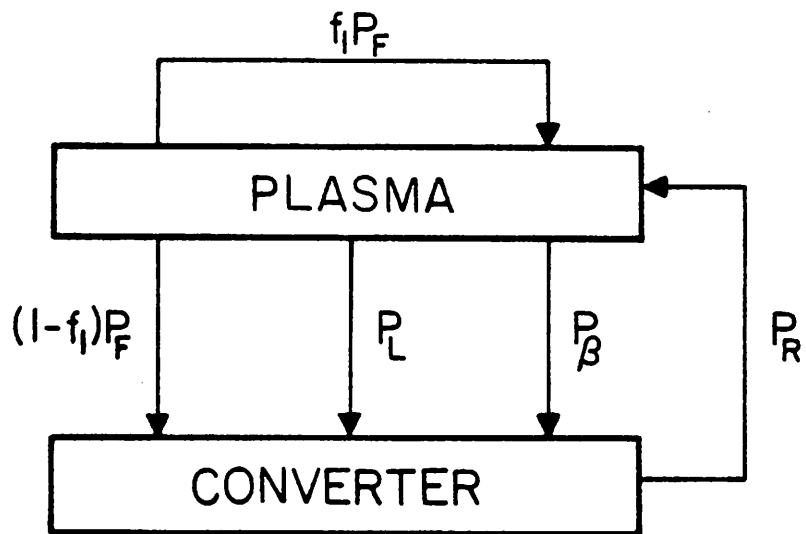
Fig. 3.   The power flows in a multiple mirror reactor.
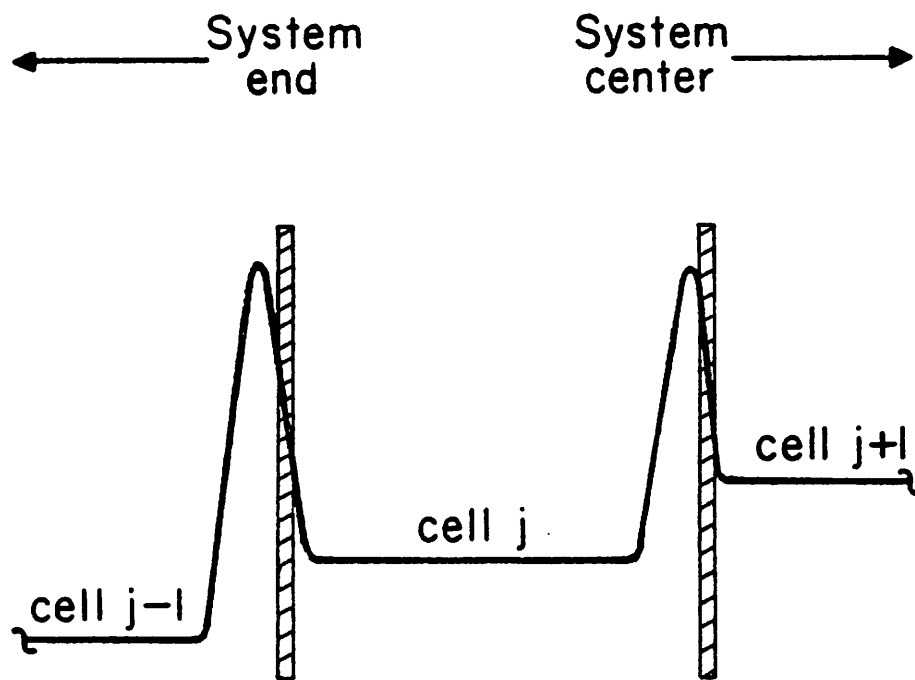
Fig. 4. The asymmetric application of ICRF. The dark bars are the resonance zones.
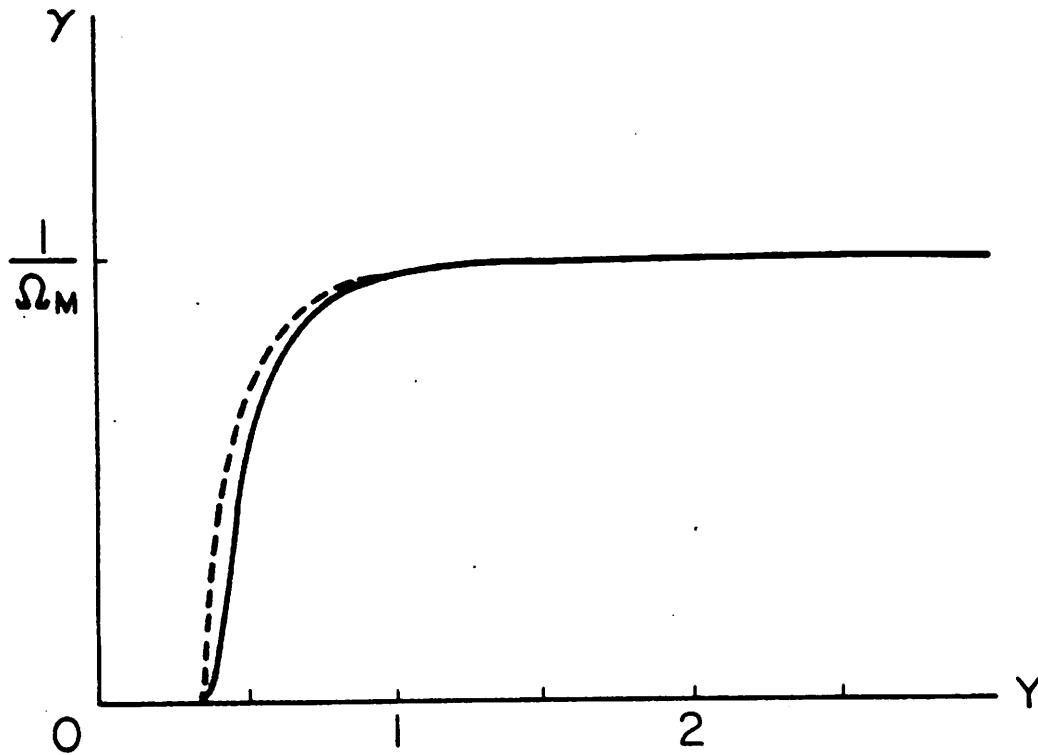
Fig. 5. The solid line is the loss cone edge generated by numerical integration of the known terms of equation (36). The dashed line is the loss cone edge generated by equation (37).
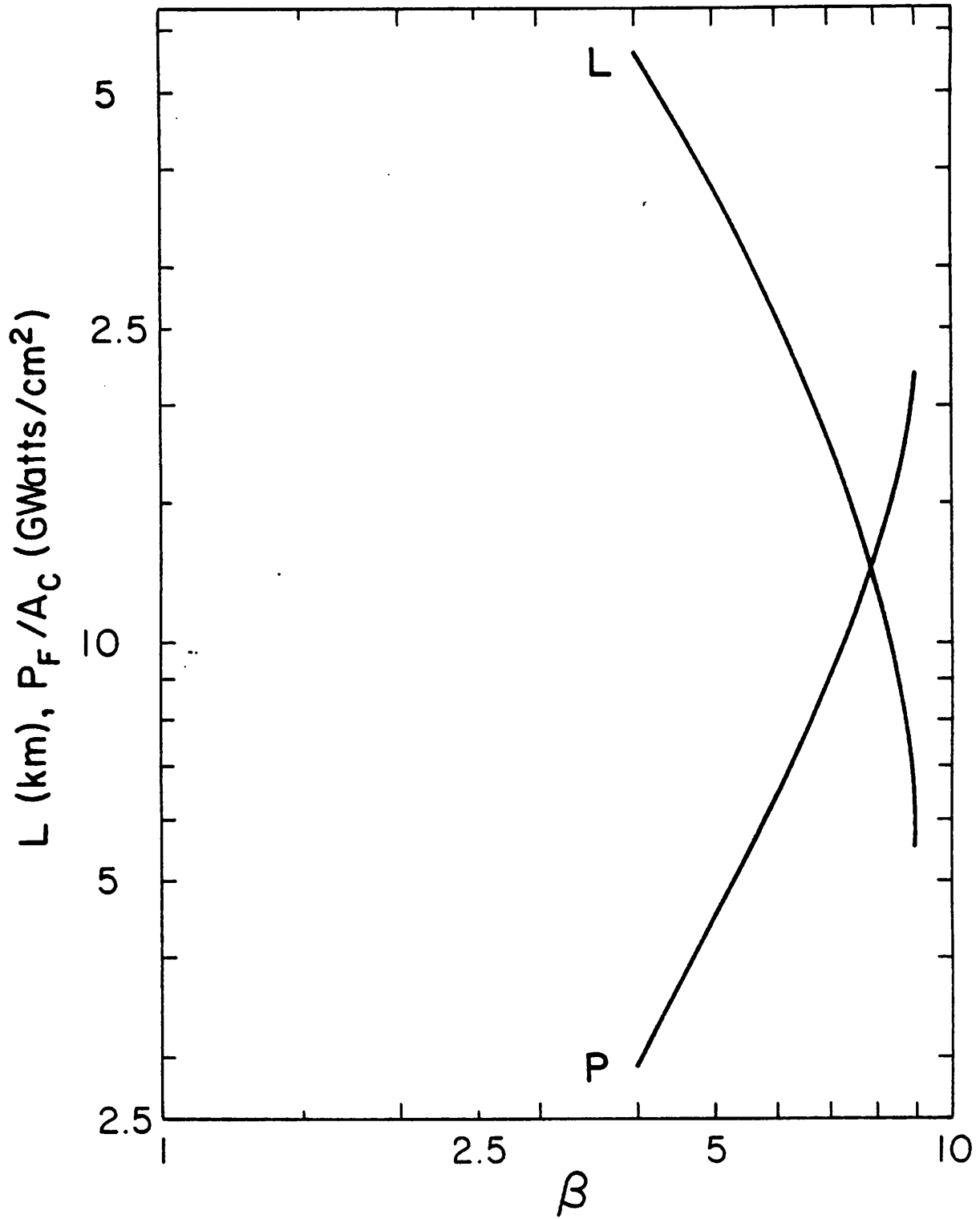
Fig. 6. System length ("L") and fusion power density ("P") versus β

for the system with no ICRF.
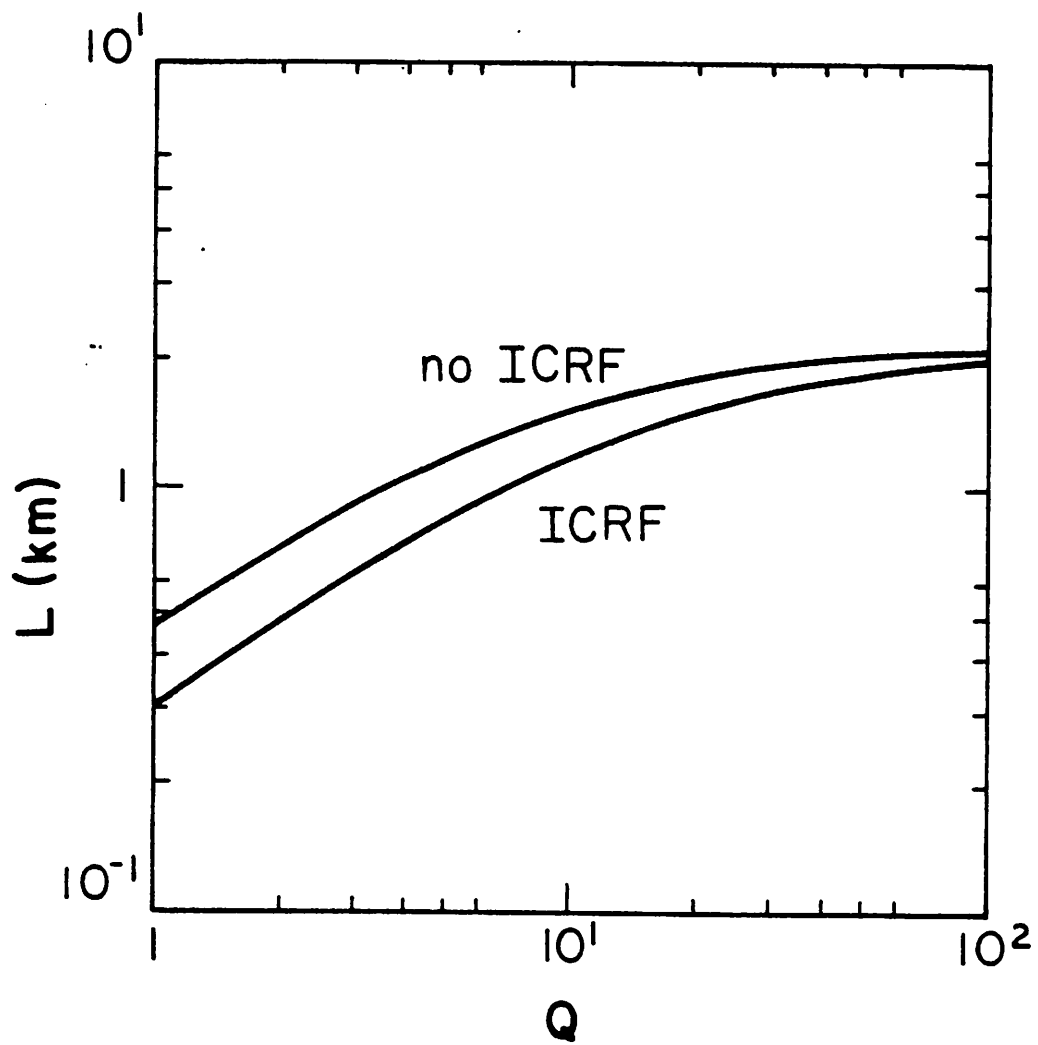
Fig. 7. L versus Q for a system with no ICRF and a system with ICRF.
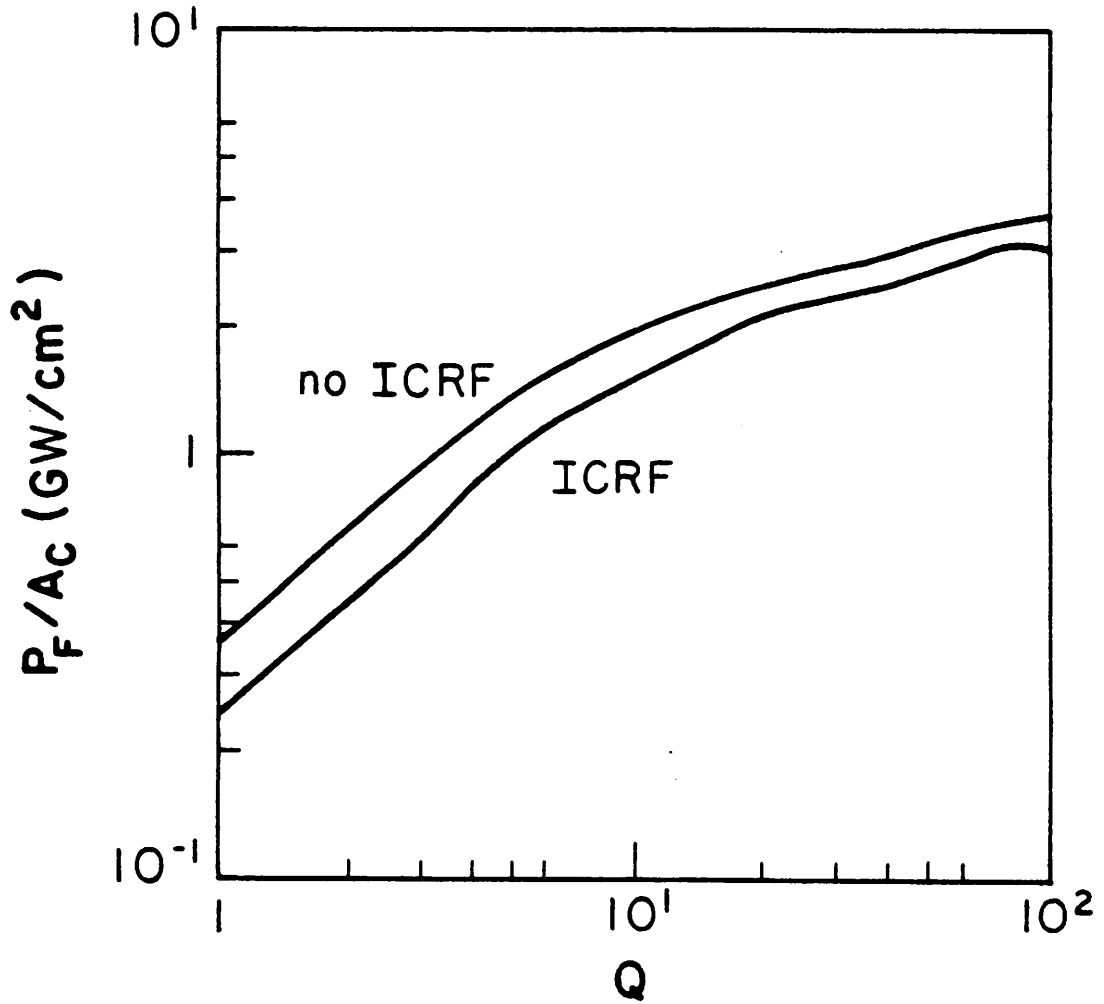
Fig. 8. P_F/A_C versus Q for a system with ICRF and a system without ICRF.
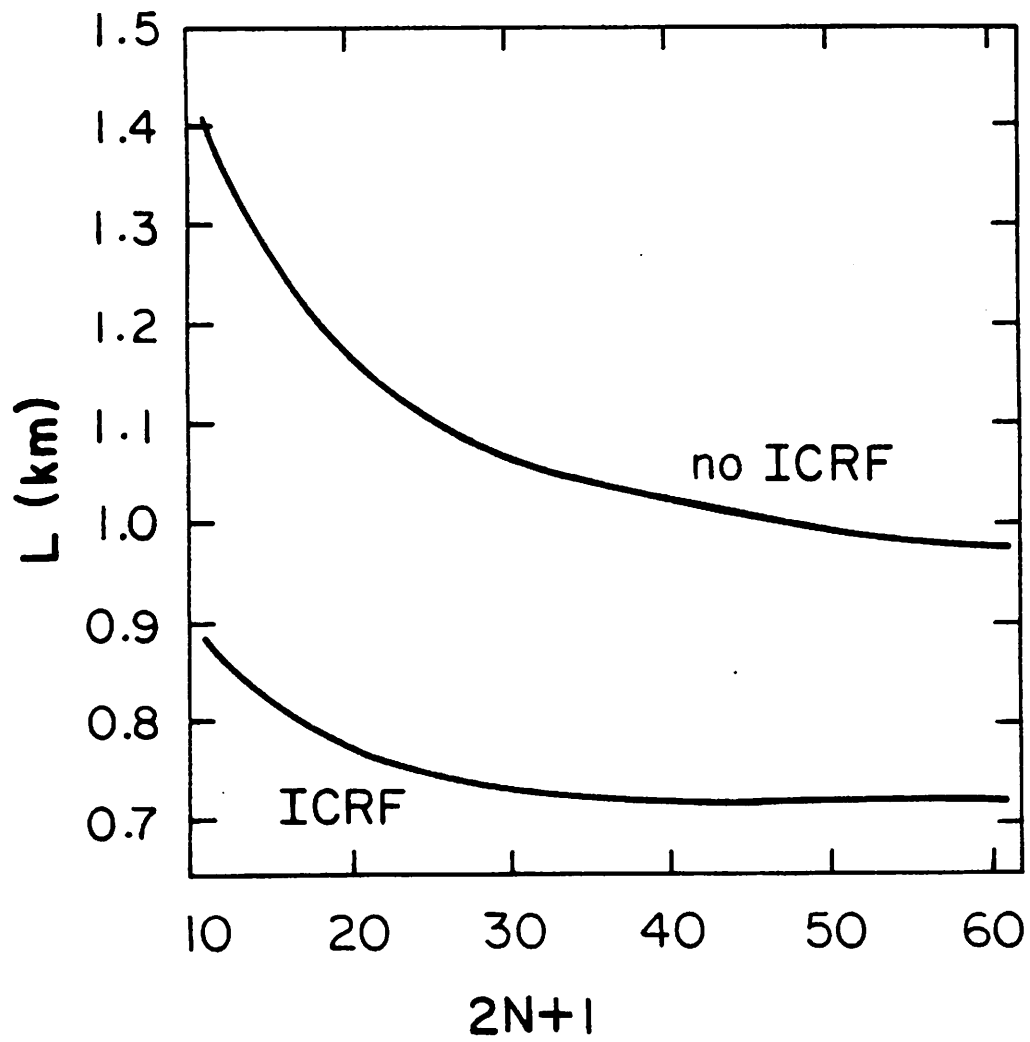
Fig. 9. L versus 2N+1 for a system without ICRF and a system with ICRF.
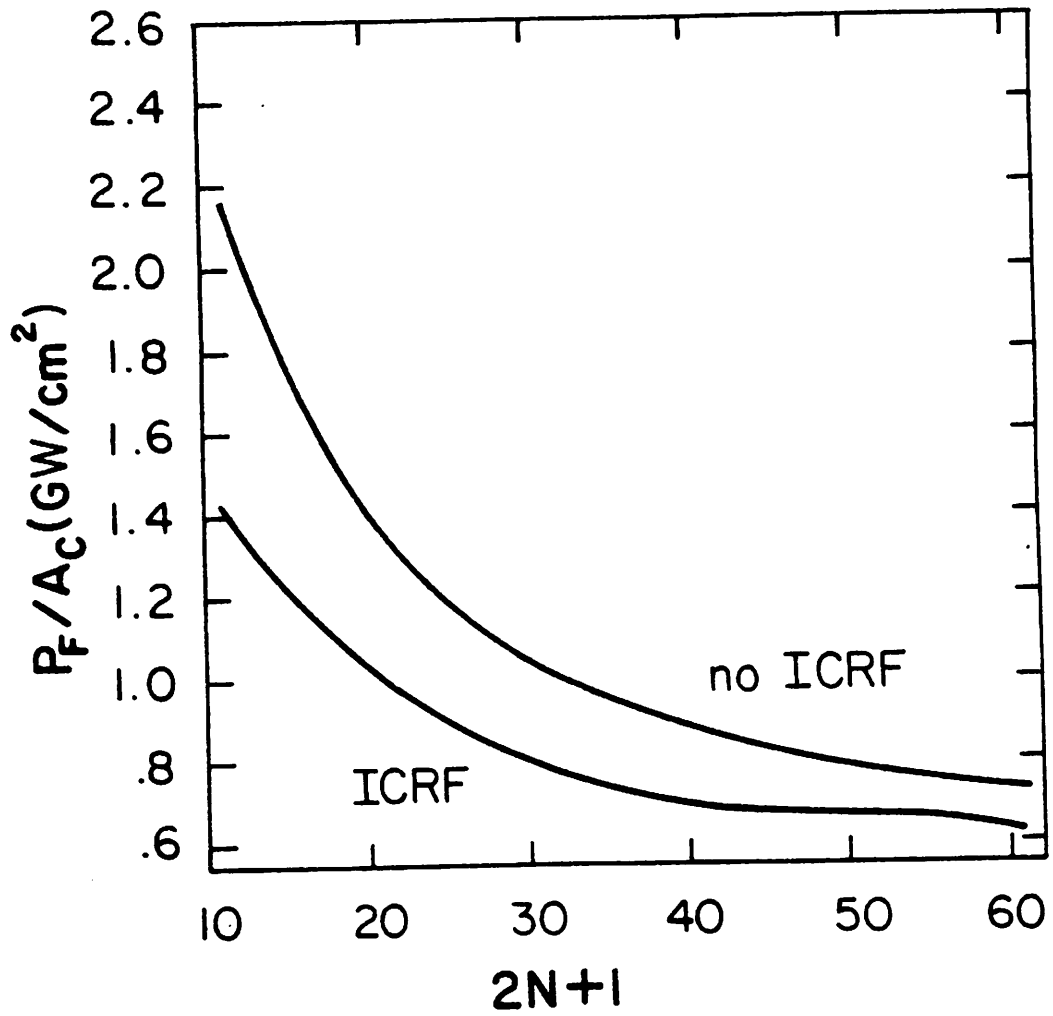
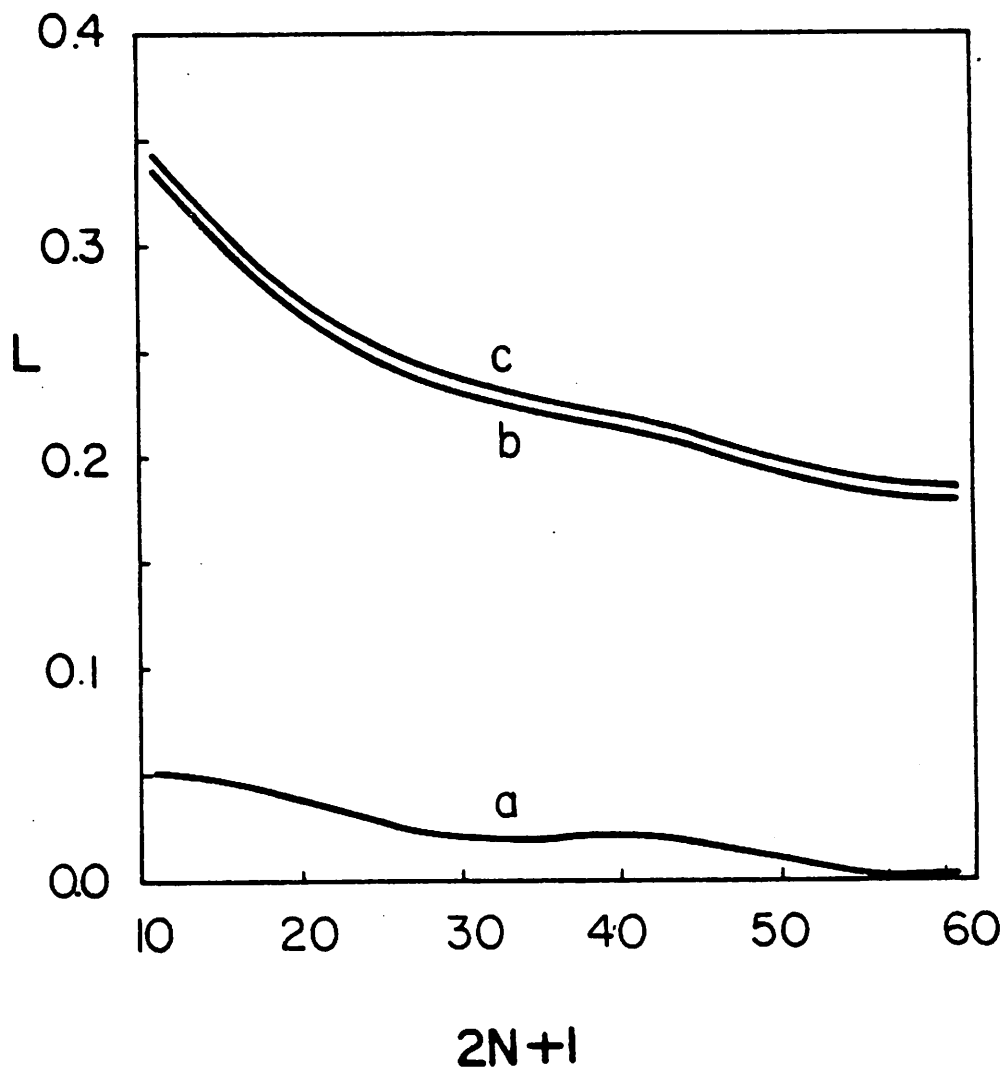Fig. 10. P_F/A_C versus 2N+1 for a system without ICRF and a system with ICRF.

Fig. 11. Fractional reduction in L versus 2N+1. A system with symmetric
ICRF "a," a system with asymmetric ICRF but without ICRF
scattering "b," and a system with asymmetric ICRF and scattering
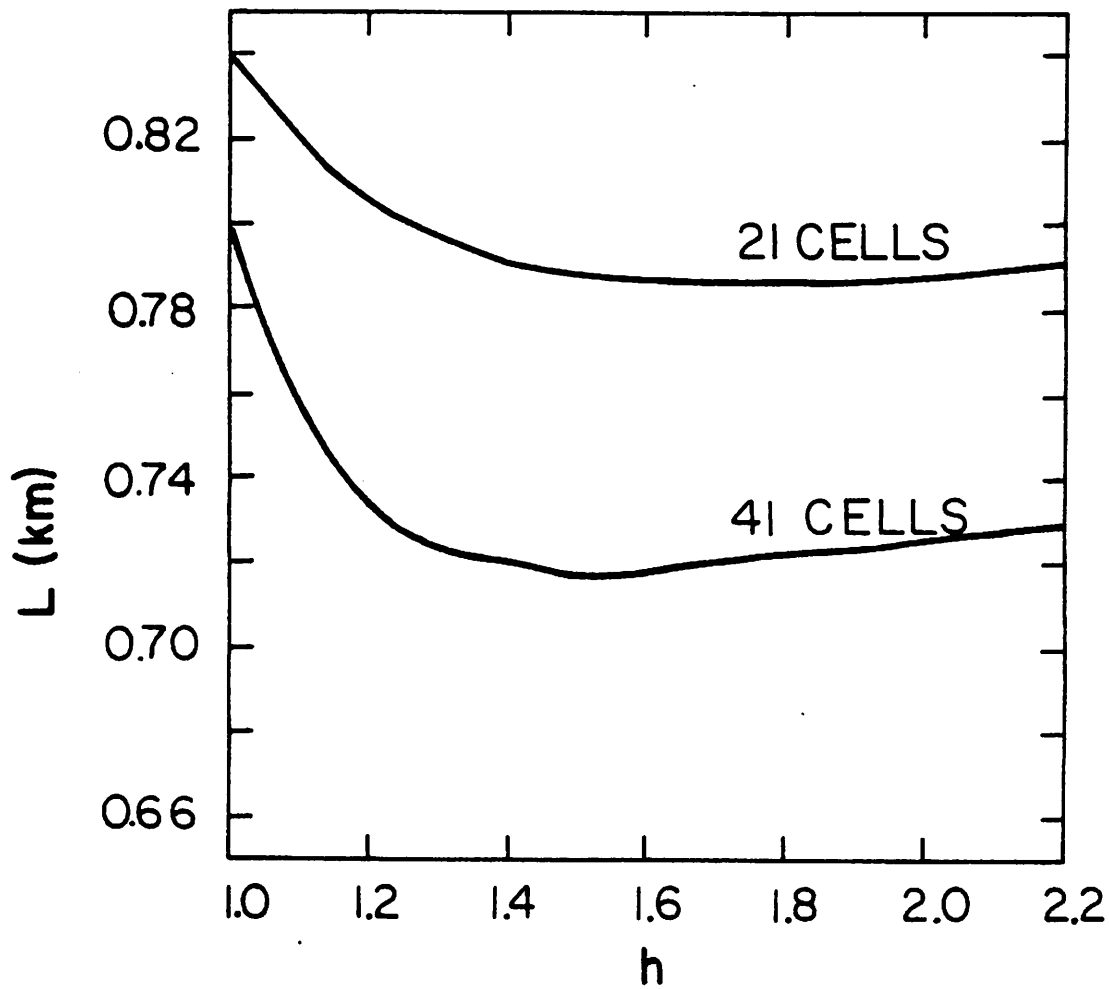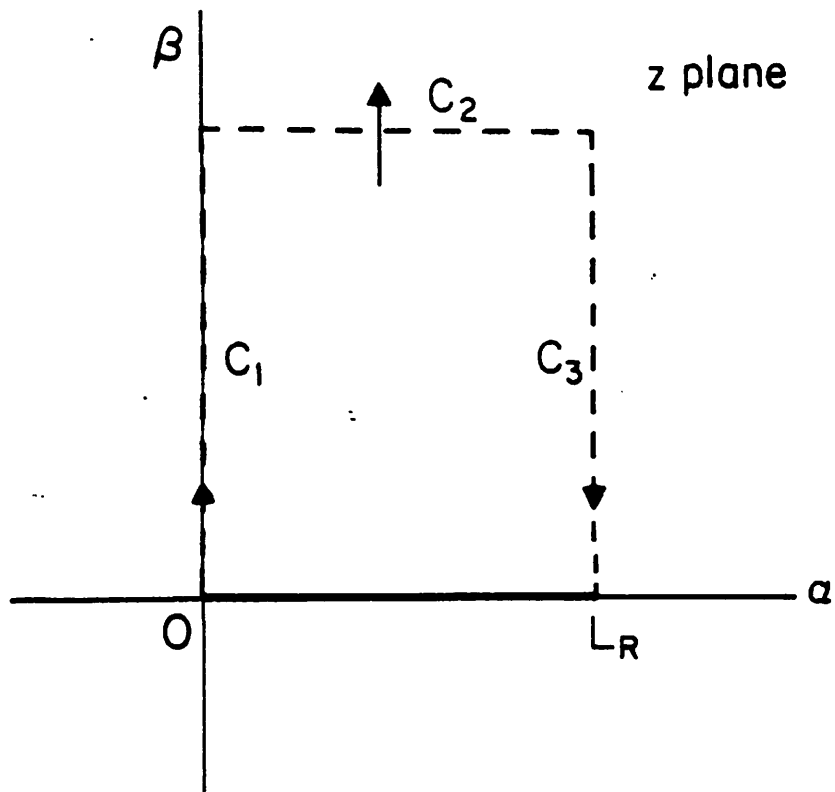"c."

Fig. 12.   L versus h.

Fig. 13. The complex z plane, showing contours. The original contour (solid line) is deformed to the dashed line.